metals

MDPI

Article

Rheo-Diecasting of Wrought Magnesium AZ31 Alloy and the Effect of Injection Velocity on Microstructure and Tensile Strength

Zelin Jin [1], Bo Xing [1,*], Chengli Tang [1], Junyan Feng [2], Na Su [3] and Yuandong Li [4]

[1] College of Mechanical and Electrical Engineering, Jiaxing University, Jiaxing 314001, China; jzl847424@163.com (Z.J.); tcl-lily@mail.zjxu.edu.cn (C.T.)
[2] NanHu College, Jiaxing University, Jiaxing 314001, China; fjyjojo@163.com
[3] Applied Technical School, Jiaxing University, Jiaxing 314001, China; suna9180@gmail.com
[4] State Key Laboratory of Advanced Processing and Recycling of Non-ferrous Metals, Lanzhou University of Technology, Lanzhou 730050, China; liyd_lut@163.com
* Correspondence: xingbo@mail.zjxu.edu.cn; Tel.: +86-137-3825-0497

Received: 25 September 2018; Accepted: 1 October 2018; Published: 3 October 2018

Abstract: Wrought Mg AZ31 alloy was near-net-shaped by semisolid rheo-diecasting. Parts with 42% and 61% solid fraction were produced at different injection velocities. The impact of injection velocity on the microstructure and the tensile strength of samples have been investigated. Results indicated that the shape factor and the particle size of primary α-Mg in the microstructure decreased with the increase of injection velocity, and the morphology of both secondary α-Mg and eutectic α-Mg + $Mg_{17}Al_{12}$ mixture were refined with the increase of injection velocity. The surface liquid segregation in the sample closely relates to the injection velocity and the solid fraction of slurries, and it decreased with the increase of injection velocity and the decrease of the solid fraction. Cold shut, crack, and gas porosity were the main internal defects that rely on the injection velocity. The tensile strength of the samples decreased with the increase of injection velocity, and the best value of 201 and 192 MPa was obtained at 0.5 m/s and 1 m/s for the sample with the solid fraction of 0.61 and 0.42, respectively. This work demonstrated a predominant effect of internal defects on the property of the rheo-diecasting (RDC) product than the microstructure; thus, defect reduction should be preferentially considered in the optimization of the RDC process.

Keywords: semisolid; AZ31 alloy; rheo-diecasting; injection velocity; microstructure; tensile strength

1. Introduction

Semisolid forming (SSF) uses metal slurry containing a certain fraction of the fine and spherical solid phase as the initial material for mold forming. Due to the non-dendritic solidification mode of the metal alloy in SSF, this technology offers a series of advantages compared with traditional cast and plastic forming, such as improved metal fluidity, reduced deformation resistance, integrity microstructure, and the fine properties of products [1]. Nowadays, because SSF offers a promising way to solve problems that are encountered by conventional shaping of wrought alloys such as the poor castability and the cast defects, many studies have been focused on the manufacturing of wrought alloy components by SSF [2–4].

Wrought magnesium such as Mg–Al series alloys has broad application prospects in the industry of aerospace, and vehicle and consumer products, because of the advantages of low density, high specific strength, and good dimensional stability [5]. Casting these alloys directly into net shape components by using SSF technology has many economic benefits. Zhen et al. investigated the semisolid rheo-diecasting (RDC) of the AZ61 alloy, and demonstrated that RDC imparts excellent

properties and high integrity to this alloy, while retaining all of the advantages of high pressure die casting, although this wrought alloy has been treated as not being suited to die-casting [6]. Guan et al. produced a non-dendritic slurry of the AZ31 alloy, and directly cast this slurry into strip by using a rheo-rolling process. Results indicated that the product has a good quality surface and a homogenous microstructure [7]. Meng et al. investigated the non-dendritic microstructure evolution of an AZ31 alloy during semisolid reheating, and developed the optimum reheating parameter for the microstructure spherioidization of this alloy [8]. However, until now, little work has been discussed for the microstructure and the tensile properties of the rheo-diecast-wrought Mg product as the effect of processing parameter, especially the alloy with low Al content. In this paper, the wrought Mg AZ31 alloy was used as the material for the rheo-diecasting experiment, for the first time. A semisolid slurry of this alloy was cast by high pressure die-casting at different injection velocities, and the effect of injection velocity on the microstructure and tensile strength of the samples has been studied. This work established a connection between the processing parameter of the injection velocity and the microstructure and tensile strength of the rheo-diecast AZ31 alloy, and this is of practical significance in the establishment of processing parameters in rheo-diecasting of wrought Mg alloys.

2. Materials and Methods

The composition of the AZ31 alloy used was: Al 3%, Mn 0.6%, Zn 1%, Cu 0.05%, Si 0.1%, Mg balance (Ningxia Huayuan MagnesiumIndustry Group Co., Ltd., Ningxia, China). The RDC experiment included semisolid slurry preparation and die-casting. The slurry was prepared with a self-inoculation method, which involves adding certain fraction of solid blocks of AZ31 and pouring the alloy melt through a multi-stream cooling channel. Details of this process are shown in the literature [9,10]. In this work, 1.5 kg of alloy ingots was melted in a resistance furnace. After preparation, the slurry was transferred to a cold chamber high-pressure die-casting machine (DAK450-54RC, FRECH Die Casting Machine Co., Ltd. Shanghai, China) and die-cast at different injection velocities from 0.5–9 m/s. It should be emphasized that this velocity range was selected as a value that can ensure the complete filling of the slurry, and so the lowest velocity of 0.5 m/s was employed. A mold temperature controller (ROBAMAT 5212, FRECH Die Casting Machine Co., Ltd., Shanghai, China) was used to control the mold temperature at 250 °C, and the boost pressure of the die casting machine was set steadily at 160 MPa. Slurries with a solid fraction of 0.42 and 0.61 were employed for the RDC experiments.

The rheo-diecasting product contained a biscuit, a cross and inner gate, an air vent and four sheet samples, as shown in Figure 1. The sample for microstructure examination, as marked in Figure 1, was cut from the center of the sheet sample along the axial line. The cross-sections was polished and etched with 10% HCl solution. The center of these samples was observed with an optical microscope (OM, NIKON Instruments (Shanghai) Co., Ltd., Shanghai, China). Macroscopical distribution of the semisolid microstructure was observed with a video microscope (GR001-200HD, Shanghai Gold Room Co., Ltd., Shanghai, China). A scanning electron microscope (SEM, NEC Electronics Corporation, Tokyo, Japan) was used for observing the secondary solidification microstructure of samples. Quantitative examinations of the OM micrographs were carried out by using Image-Pro plus software (6.0, Sino-Vision Technology Co., Ltd., Beijing, China). The average particle size and shape factor of the primary phase were respectively calculated using the following equations: $D = 2(A/\pi)^{1/2}$, $F = P^2/4\pi A$, where A and P are the area and perimeter of the solid particle, respectively. Tensile strength was tested at room temperature by a material testing machine (WDW-100D, Yangzhou Sankun Instrument Equipment Co. Ltd., Yangzhou, China), and the strain rate was 0.5 mm/s. The average value of the three tensile samples was used as the strength value. A scanning electron microscope (SEM, Hitachi Co., Ltd. Tokyo, Japan) was used for fracture surface observation.

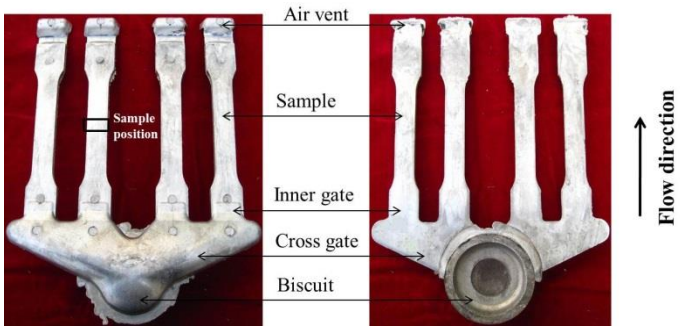

Figure 1. Photograph of the RDC product.

3. Results and Discussion

3.1. Thermodynamic Characteristics of the AZ31 Alloy Used for Rheo-Diecasting

In order to develop an essential thermodynamic guide for semisolid processing, thermodynamic simulation of the phase diagram of AZ31 alloy was first carried out by using the pandat software package (version 7.0, Compu Therm LLC, Middleton, WI, USA). This calculation was based on the composition of the AZ31 alloy shown in Section 2. Figure 2 shows the temperature versus solid fraction curves obtained using the lever rule and the Scheil equation. It can be found that the solidification temperature range of this alloy (from liquidus to solidus) is 180.32 °C (673.17−492.85 °C) for the lever rule model, and the 335.03 °C (673.17−338.13 °C) for the Scheil equation model. The precipitation temperature of the primary α-Mg phase has only a tiny difference between the two models, which is 630.82 °C for the lever rule and 630.72 °C for the Scheil model. However, the changing trend of temperature with the solid fraction in these two models becomes more and more diverged along with the solidification. The obvious discrepancy is that in the Scheil equation, the eutectic reaction appears, but in the lever rule model, the eutectic reaction does not appear. Considering that the alloy experiences non-equilibrium solidification in actual rheo-diecasting, the calculation result based on the Scheil model was adopted. Referring to this result, the slurry temperature was set steadily and exactly at 620 °C and 610 °C in the RDC experiment, and the corresponding solid fraction was 0.42 and 0.61 respectively.

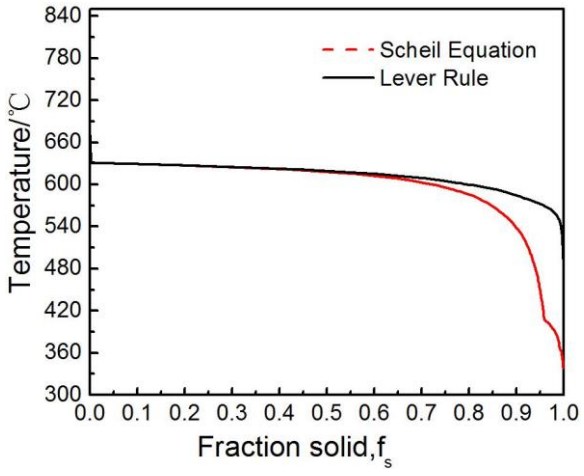

Figure 2. Temperature vs solid fraction curves of the AZ31 alloy, obtained by thermodynamic simulation with the lever rule and the Scheil equation.

Figure 3 shows the precipitation sequence and the molar fractions of all solidified phases during the non-equilibrium solidification of AZ31. The main elements such as Mg, Al, Mn, and Si were used for the thermodynamic simulation, while the other elements were omitted due to their negligibility.

It can be found that the hard Al_8Mn_5 phase was initially formed along with melt cooling, then α-Mg (HCP), Mg_2Si, and $Al_{11}Mn_4$ were formed in order with the decrease of temperature. The γ-$Mg_{17}Al_{12}$ phase finally formed from an eutectic reaction, indicating the finishing of solidification.

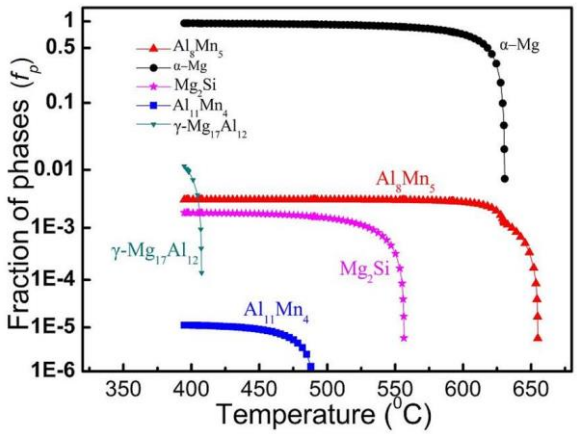

Figure 3. Precipitation sequence and molar fractions of all solidified phases during the non-equilibrium solidification of the AZ31 alloy.

3.2. Slurry Microstructure of the Semisolid AZ31 Alloy

In order to investigate the semisolid microstructure feature of AZ31, the microstructure of the samples quenched at 610 °C in different solidification conditions were examined. As shown in Figure 4a, the sample microstructure from conventional solidification presented a coarse dendritic structure, and the average size of the primary α-Mg was up to 413 μm. In Figure 4b, the melt was internal chilled with alloy blocks and then poured through a multi-stream cooling channel. The microstructure consisted of fine and spherical α-Mg particles, and its average size was reduced to 76 μm. This semisolid microstructure feature, similar to cast Mg alloy of high Al content such as AZ91 and AM60 [11,12], commendably meets the requirements of semisolid forming. The authors' previous work provides detailed information of the slurry-making process [9,10].

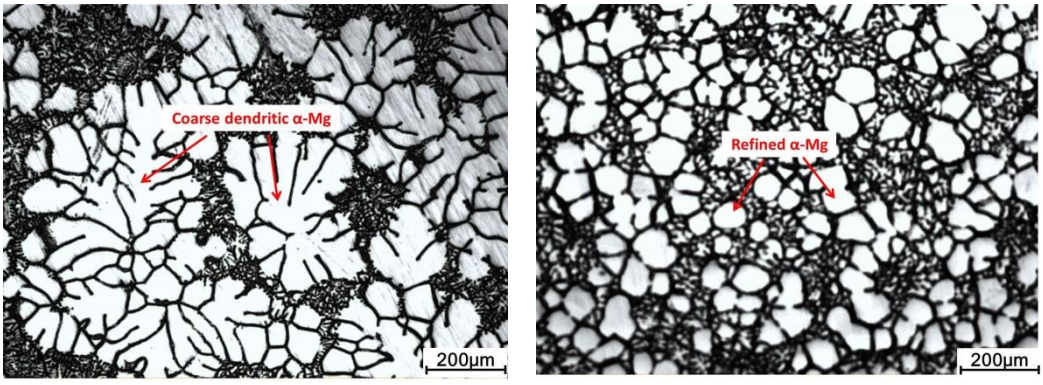

(**a**) (**b**)

Figure 4. Microstructure of semisolid AZ31 alloy quenched at 610 °C. (**a**) Conventional solidification; (**b**) after the slurry preparation procedure.

3.3. Effect of the Injection Velocity on Microstructure

Figure 5 shows the microstructure of the rheo-diecasted AZ31 alloy at different injection velocities. When the velocity was 0.5 m/s, Figure 5a, the primary α-Mg in the sample with a solid fraction of 0.42 were mainly spherical particles, and a small quantity of rosettes were occasionally observed. In addition to the non-dendritic form of the α-Mg particles, there were some protuberances on the particle surface, tiny dendrites, and very fine α-Mg particles existing in the microstructure. These grains were formed in

the chamber and in the die cavity during solidification of the remaining liquid, and they accounted for a small proportion in the microstructure [6]. When the injection velocity was increased to 1 m/s, more individual grains appeared as spherical particles, and the surface protuberance on the particle surface was evidently reduced. Similarly, some dendrites still existed between the primary phases, as shown in Figure 5c. A further increase of velocity to 3 m/s (Figure 5e) led to a significant change in the shape of the particles, with the rosettes almost changed into spherical particles and with most of the primary phase becoming rounder. Comparing Figure 5b,d,f reveals that in the sample with the solid fraction of 0.61, when the velocity was increased from 0.5 m/s to 3 m/s, more neighboring grains changed into separate grains, and the morphology became rounder. Differently, dendrites in the liquid matrix were significantly reduced, even at a low velocity of 0.5 m/s (Figure 5b).

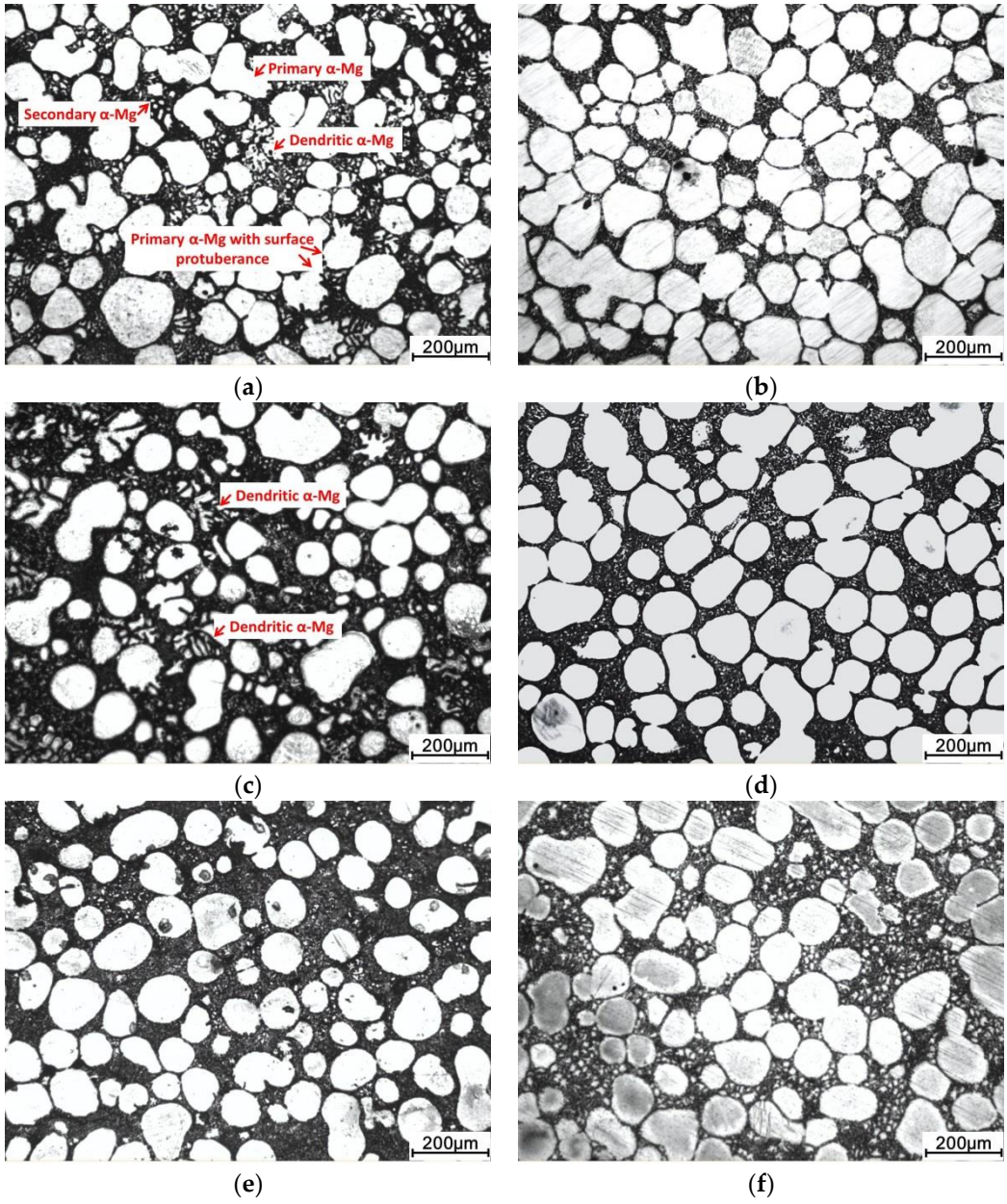

Figure 5. Microstructure of the rheo-diecast AZ31 alloy with different solid fractions of 42% (**a**,**c**,**e**) and 61% (**b**,**d**,**f**) under different injection velocities. (**a**,**b**) 0.5 m/s; (**c**,**d**) 1 m/s; (**e**,**f**) 3 m/s.

Figure 6 shows the effect of injection velocity on the particle size and shape factor of the primary α-Mg particles. The size and shape factor of the primary α-Mg in slurry before die-casting has also been

analyzed by observing the microstructure of the quenched sample. It can be found that the die-casting process had a promoting effect on the reduction of the particle size and shape factor, especially at a high injection velocity. Furthermore, the particle size in these two solid fraction conditions all decreased with the increase of injection velocity, and the shape factor decreased as well. It was also found that the primary α-Mg particles at the solid fraction of 0.61 were larger and rounder than the solid fraction of 0.42. This means that the growth and the coarsening of primary α-Mg were prolonged with the cooling of slurry from 620 °C to 610 °C. From these results, it is reasonable to conclude that the high injection velocity is beneficial to the grain refinement and the spheroidization of the primary phase in RDC.

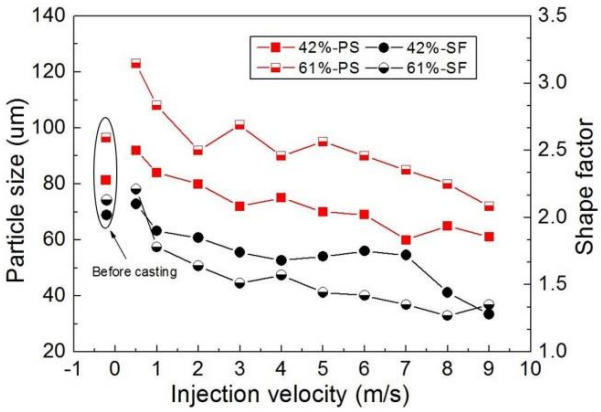

Figure 6. Effect of injection velocity on the particle size and the shape factor of primary α-Mg in rheo-diecast AZ31 alloy under different solid fractions.

In RDC, the final morphology of primary α-Mg is determined by grain nucleation and growth occurred in both the slurry preparation and the die-casting stage [13]. In slurry preparations, the individual grains come from single nucleation and dendrite fragmentation [14]. These grains tend to retain their morphology in die-casting. However, the injection velocity has a significant effect on slurry cooling and flow behavior in forming. According to Hamasaiid et al., with the increase of velocity, the interfacial heat transfer coefficient at the metal–die interface was increased. Thus, the temperature gradient of the surface and at the central part of the casting was increased, resulted in an increase of cooling rate [15]. This is beneficial to promote the solidification rate and to inhibit the growth of the primary phase. Moreover, a high injection velocity also means a more intense shearing force between the slurry and mold wall, thus giving rise to particle collision and abrasion. This is able to form dendrite fragments and to promote grain multiplication [16]. In addition, the friction heat in the melt was also an outcome of the intensive shearing at high velocity, which was a potential factor for separating the rosette particles from their neck, and contributing to the refinement of primary α-Mg [17].

Figure 7 shows the microstructures of the matrix between primary α-Mg particles. This microstructure was formed from the solidification of remaining liquid in the die cavity (which also can be termed as secondary solidification [18]). At the solid fraction of 0.42 and the velocity of 0.5 m/s, Figure 7a, the ramiform protuberances attached on the primary α-Mg surface and many dendrites existed in the matrix. This indicates that the remaining liquid was nucleated both on the surface of primary phase and within the liquid matrix. As the velocity was increased to 3 m/s, Figure 7b, the protuberances on the primary α-Mg reduced and the dendritic α-Mg evolved into coarse granular particles. This implies that with the increase of velocity, the nucleation occurred mostly within a liquid matrix, and the secondary solidification microstructure was refined. The same results can be found in samples with 61% solid fraction when comparing Figure 7c,d. A distinction is that the secondary α-Mg in Figure 7d were more fine and uniform compared with Figure 7b, which indicates a more remarkable refining effect of high velocity on the secondary solidification microstructure at a high solid fraction.

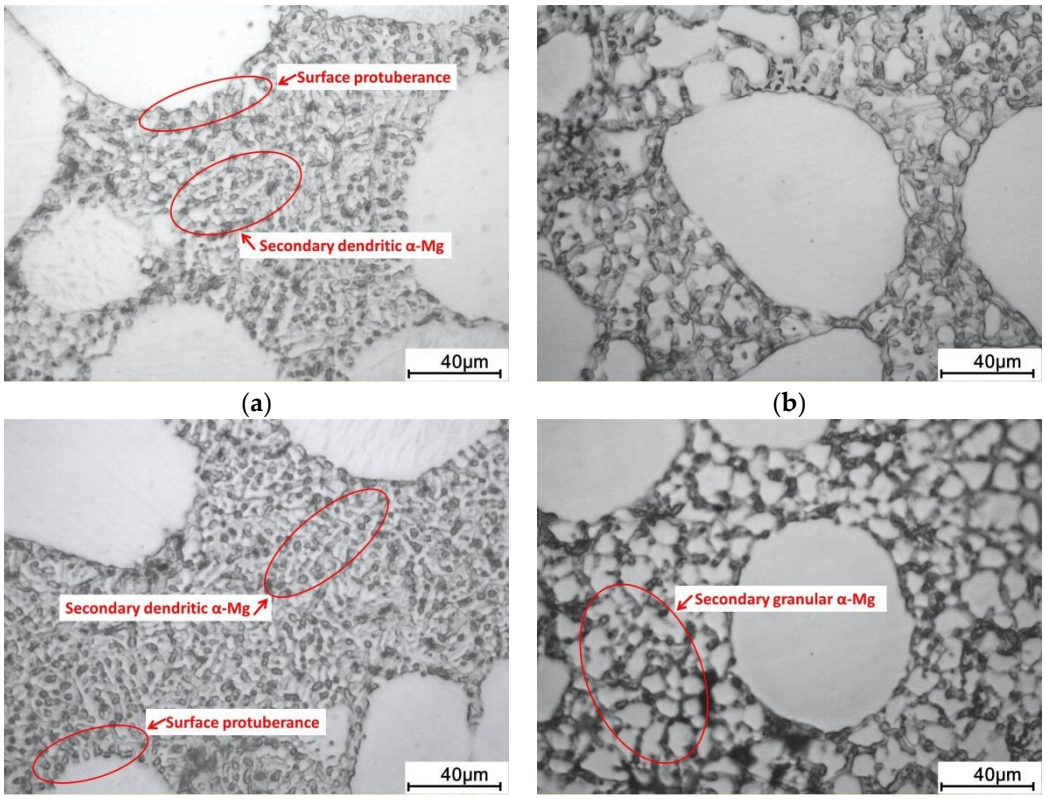

Figure 7. Solidification microstructure of the remaining liquid in rheo-diecast AZ31 alloy with a solid fraction of 42% (**a**,**c**) and 61% (**b**,**d**) under different injection velocities. (**a**,**b**) 0.5 m/s; (**c**,**d**) 3 m/s.

Figure 8 shows the SEM photograph of the secondary microstructure. The grey and white phases indicated by the arrow are the eutectic α-Mg + $Mg_{17}Al_{12}$ mixtures formed at the end of solidification. At the velocity of 0.5 m/s, when the solid fraction was 0.42 (Figure 8a), the eutectic mixture was present as island shape, and most of it was centered around secondary α-Mg particles. As the solid fraction was increased to 0.61 (Figure 8c), the agglomeration of the eutectic mixture was reduced, but it was still visible in some regions. In the Mg–Al alloy, the brittle $Mg_{17}Al_{12}$ phase always acted as an initiation site for cracks; thus its agglomeration had a negative impact on the product properties [19]. When the velocity was increased to 3 m/s, it was evident from Figure 8b and d that the eutectic mixture evolved to discontinuous strips and fine granular structures, and its distribution became more disperse, especially in the sample with a solid fraction of 0.61 (Figure 8d). It is therefore evident that the high injection velocity was also beneficial to the refinement of eutectic phase. As mentioned above, the high cooling rate of the slurry in the die cavity, induced by an increased injection velocity, was beneficial to induce immediate heterogeneous nucleation of the secondary α-Mg, and thus gave rise to a fine and granular morphology of the secondary α-Mg. On another hand, according to Fan et al., the high injection velocity gave rise to melt turbulence; thus, the solutal diffusion boundary layer thickness around a growing solid could be reduced, therefore promoting the spherical growth of secondary α-Mg [20]. Due to this refining effect, the liquid along the solid boundaries presented as a thin film rather than liquid pools between dendrites. These liquid films finally solidified into a fine and dispersive eutectic mixture, thus producing a refined eutectic structure.

The distribution of the primary phase, namely the macrostructural uniformity, is also an important factor effecting the final property of the castings [21,22]. Therefore, the distributions of primary α-Mg in the cross-sections of the samples have also been investigated. Figure 9 shows the distribution of the primary α-Mg in entire cross-section of the sample, with a solid fraction of 0.61 and an injection velocity of 1 m/s. It is obvious that a solid segregation layer appeared on the sample surface, and this

was nearly symmetrical in the channel. In the experiment, we found that this segregation within the same sheet sample was nearly changeless along the flow direction.

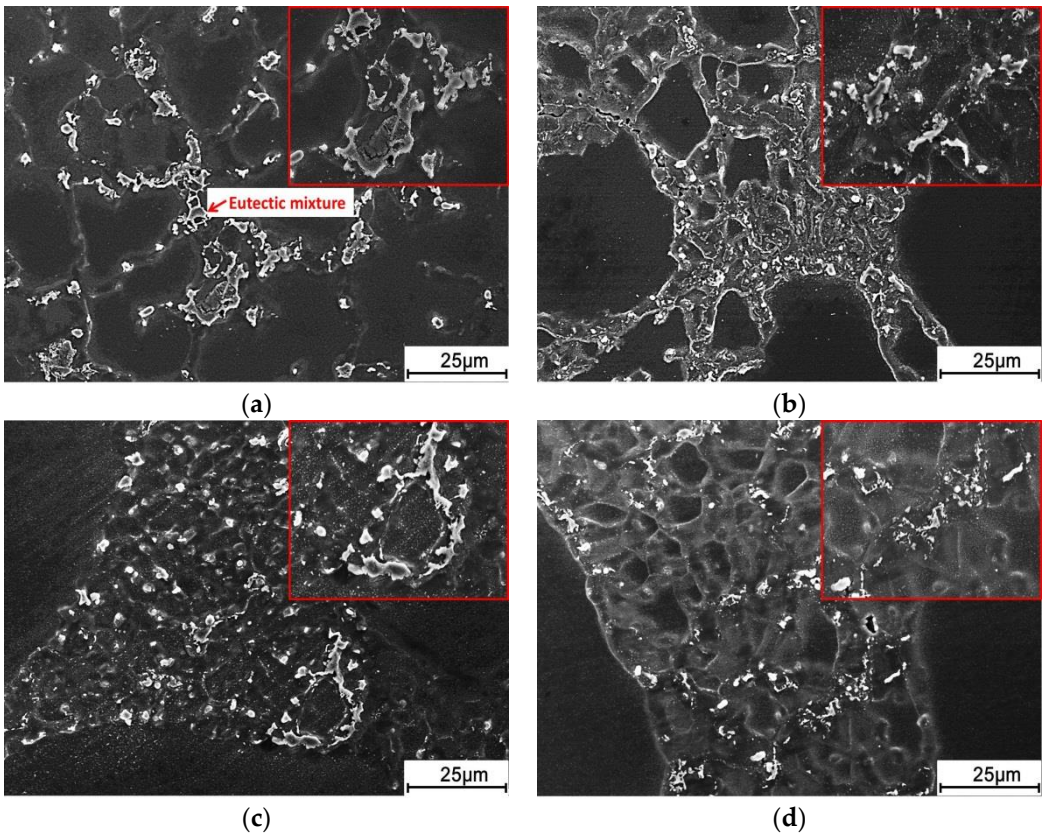

Figure 8. SEM pictures of secondary solidification region in rheo-diecast AZ31 alloy, with solid fractions of 42% (**a**,**c**) and 61% (**b**,**d**) at different injection velocities. (**a**,**b**) 0.5 m/s; (**c**,**d**) 3 m/s.

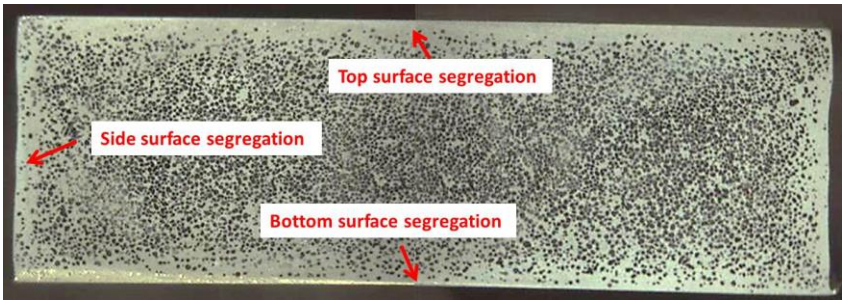

Figure 9. Distribution of primary α-Mg in entire cross-section of the sample.

Figure 10 show the effect of the solid fraction and the injection velocity on this surface segregation. In Figure 10a, under a solid fraction of 0.42 and an injection velocity of 0.5 m/s, the α-Mg fraction gradually decreased from the center to the sample surface; thus a surface liquid layer with a width of approximately 0.3 mm formed. At the same velocity, when the solid fraction was increased to 0.61 (Figure 10c), a more serious α-Mg segregation along the sample thickness formed, and the width of the segregation layer was approximately 0.8 mm. However, when the injection velocity was increased to 3 m/s (Figure 10b), the distribution of primary α-Mg along the sample thickness became more uniform, and the surface liquid segregation was reduced readily. This is particularly evident in samples with the solid fraction of 0.61, as shown in Figure 10d.

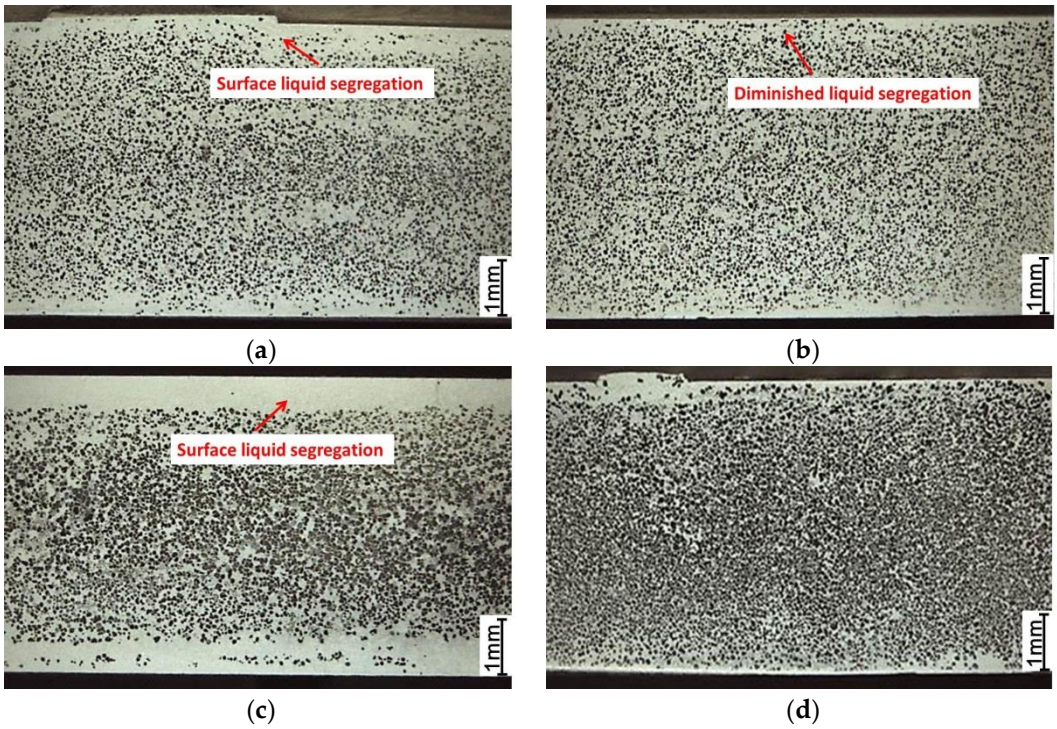

Figure 10. Macro-distribution of the primary α-Mg phase in rheo-diecast AZ31 alloy with solid fractions of 0.42 (**a**,**b**) and 0.61 (**c**,**d**) at an injection velocity of 0.5 m/s (**a**,**c**) and 3 m/s (**b**,**d**).

Figure 11 shows the variation of the primary α-Mg fraction in an area of 1 mm × 1 mm (in the center and the edge of the sample) at different injection velocities. The quantitative results revealed that at a solid fraction of 0.42, the α-Mg fraction in the sample center decreased with the increase of velocity, while the edge increased with velocity. When the velocity was larger than 3 m/s, the variation of the α-Mg fraction at the center and at the edge reached balance, and the α-Mg fraction in these two areas became equivalent. Similar results appeared at a solid fraction of 0.61. It is therefore clear that the surface liquid segregation closely relates to the injection velocity and the solid fraction, and a higher velocity is beneficial to ensuring the uniform distribution of primary phase, especially in the slurry with high solid fraction. This phenomenon is in good agreement with the results reported by Khosravani et al. and Mir et al., which refer to the microstructure of the thix-formed AZ91 and A356 alloys [23,24].

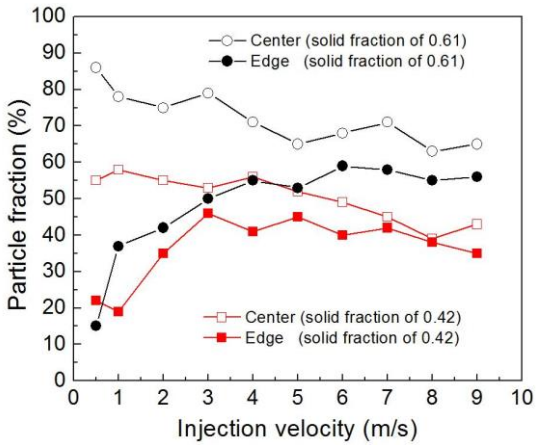

Figure 11. Variation of the primary α-Mg fraction in the center and edge of the sample with different solid fractions as the effect of injection velocity.

Theoretically, the surface liquid segregation in semisolid formed a product that can be attributed to the different fluidity of solid and liquid phases during formation. Due to the special feature of the solid–liquid mixture, the motions of solid and liquid were independent under the action of the plunger, and the velocity of the liquid phase was always higher than the solid, both of which resulted in the percolation phenomenon of the liquid within the solid–liquid mixture. As reported by Mir et al. and Vieira et al., this liquid percolation would become intensive with the increase of the solid fraction, leading to more liquid escaping from the mixture and flowing toward to the flow front [24,25]. Under the capillary force induced by the solidification shrinkage, the liquid on the flow front tended to migrate to the die wall, so as to feed the solidification shrinkage, resulting in surface liquid segregation in the sample. However, with the increase of injection velocity, the flow of the slurry during filling was more turbulent, and the liquid percolation was readily reduced, leading to the dispersive distribution of the solid phase in the bulk melt. On the other hand, the high injection velocity also means a high solidification rate, and this consequently reduced liquid migration time during die filling, with the consequence of the diminution of liquid segregation. Therefore, the distribution of the primary α-Mg phase became more uniform with the increase of injection velocity.

3.4. Effect of Injection Velocity on Defect Formation

Figure 12 shows the typical casting defects formed under different injection velocities. Figure 11a shows the internal liquid segregation occasionally observed in samples with a solid fraction of 0.42, at 0.5 m/s and 1 m/s. Different from surface liquid segregation, this defect, also called a cold shut, was formed due to liquid solidification on chamber wall or plunger surface during filling. The lower injection velocity means a longer contact time between the slurry and the chamber wall; thus, more liquid solidified in the chamber wall, and then the solidified alloy was drawn into slurry and formed the cold shut. Figure 12b shows the cracks frequently observed in the sample with a solid fraction of 0.42 when the injection was higher than 3 mm/s. Shrinkage was the main source for this crack, and this mainly resulted from insufficient solidification feeding [26]. In the later period of solidification, these cracks initiated from shrinkage and extended along the liquid matrix under shrinkage stress. Increased injection velocity means an improved solidification rate and reduced feeding time, so it was able to induce shrinkage from these cracks. Figure 12c,d show the two typical examples of the gas porosity formed at a solid fraction of 0.42 and an injection velocity of 3 m/s and 7 m/s. It was found that the size of the gas porosity decreased with the increase of velocity, but the distribution turned to be much denser. At a low velocity, the flow front presents as laminar, but some instability still exists at the semi-solid/gas interface [27], which is able to capture gas in the melt flow and form larger pores. When the injection velocity was high, the flow turned from laminar to turbulent; thus, more gas in the die cavity could be inhaled in the slurry and generate small porosities. In this work, the gas porosity was significantly eliminated at a lower injection velocity of 0.5 m/s and 1 m/s for samples with a solid fraction of 0.42 and 0.61 respectively.

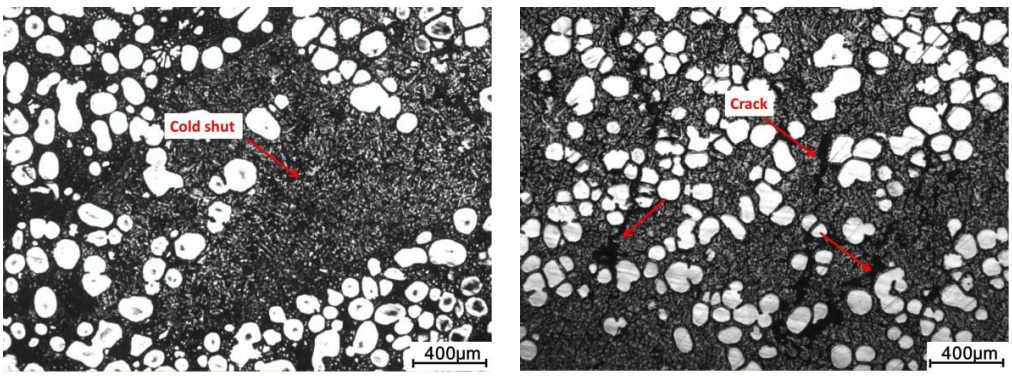

(**a**) (**b**)

Figure 12. *Cont.*

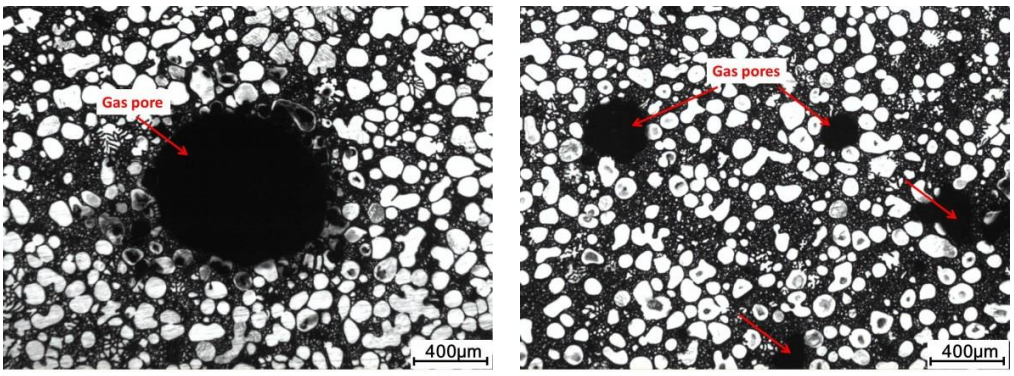

Figure 12. Internal defects in the microstructure of rheo-diecast AZ31 alloy. (**a**) Cold shut; (**b**) crack; (**c**,**d**) gas porosity.

3.5. Effect of Injection on Tensile Strength

Figure 13 shows the variation of sample tensile strength under different injection velocities. The best value of 201 MPa and 192 MPa was obtained at 0.5 and 1 m/s for samples with solid fractions of 0.61 and 0.42 respectively. Meanwhile, the strength decreased sharply along with the increase of velocity, from 1 m/s to 2 m/s. Further increases of velocity from 2 m/s to 7 m/s led to a fluctuation of the strength value, and the lowest values of 139 and 130 MPa appeared at 9 m/s and 8 m/s for the solid fractions of 0.61 and 0.42, respectively. Different from microstructure refining, this result showed an adverse effect of the injection velocity on the sample tensile strength.

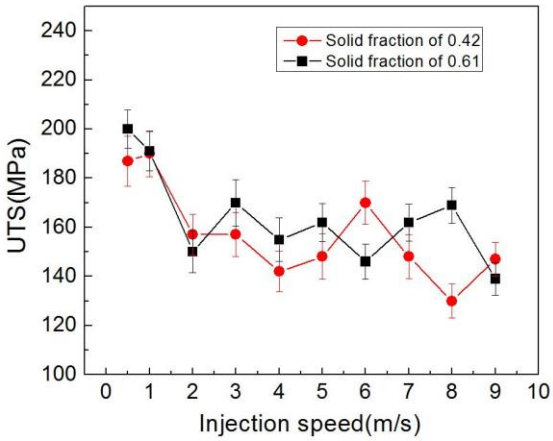

Figure 13. Effect of injection velocity on the ultimate tensile strength (UTS) of the rheo-diecasted AZ31 alloy.

Figure 14 shows the fractographs and longitudinal microstructures close to the fracture surface of the fractured sample with a slid fraction of 0.61 at 0.5 and 3 m/s. Figure 14a shows a fine-scale mixture of the transgranular cleavage plane and tear ridges which were characterized by plastic deformation. This characteristic indicates that the crack propagated both within primary α-Mg and in the fine eutectic mixture. Examination of the longitudinal sections (Figure 14c) shows the initiation of cracks within the primary α-Mg. This fracture mode is different from other rheo-diecasted Mg–Al alloys such as AZ91 and AM60. In these alloys, the fracture path was mainly along the matrix between the primary particles, due to the prevalent $Mg_{17}Al_{12}$ phase [19,28]. In Figure 14b, when the velocity was increased to 3 m/s, the fractograph exhibited some cleavage plane and the debonding between the primary α-Mg phase, and the matrix was visible. Additionally, the voids could be frequently observed in the fracture surface. The longitudinal microstructure shows that the crack was initiated on primary α-Mg surface or within the matrix. Thus, it is reasonable to assume that the porosities

such as gas porosity and shrinkage were the main factors that induced the fracture of sample. In this work, although the microstructure of sample was refined with increasing injection velocity, defects of gas porosity and shrinkage have also been formed in the samples. The negative effect of defect on sample strength exceeded the positive effect of microstructure refining and led to a decrease of tensile strength. In future work, a detailed evaluation that involves systematic changes in the volume fraction of porosity defects over a wide range of parameter conditions should be considered; this is of practical importance for developing a useful regulating model between the process parameters and the final properties of RDC products.

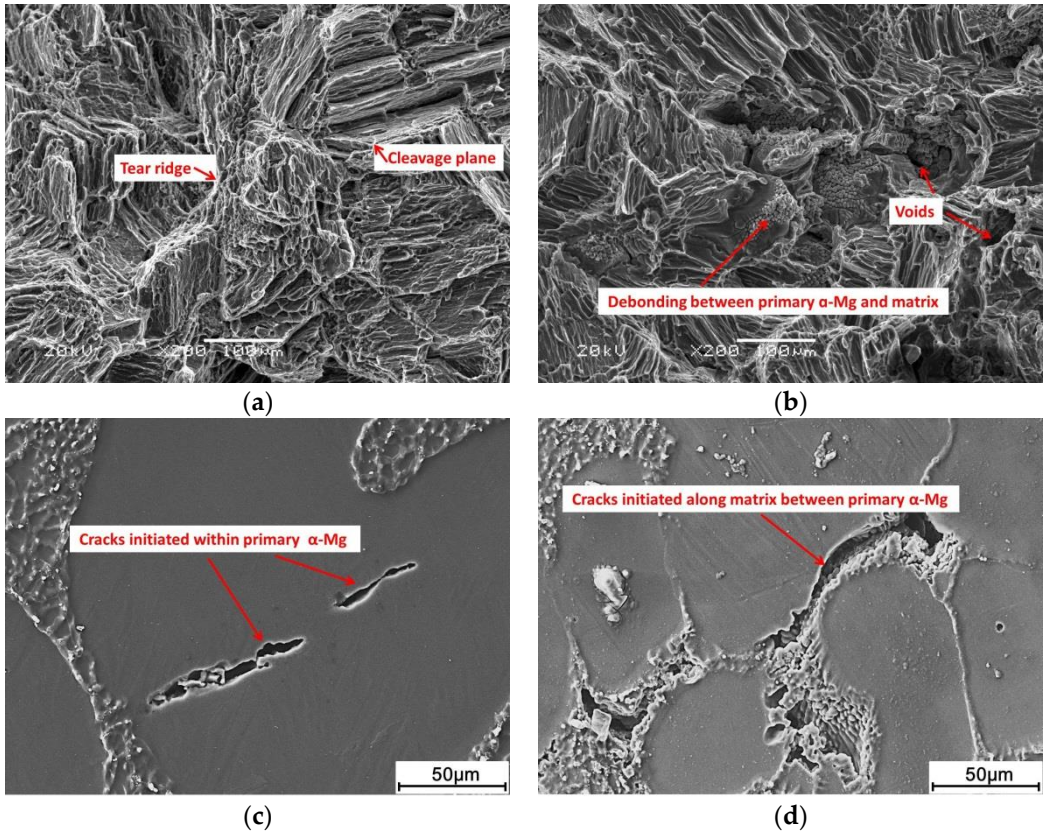

Figure 14. Fractographs (**a**,**b**) and longitudinal microstructures close to the fracture surface (**c**,**d**) of the sample with a solid fraction of 0.61 under an injection of 0.5 (**a**,**c**) and 3 m/s (**b**,**d**).

4. Conclusions

In this paper, wrought Mg AZ31 alloy was used as an experiment material for rheo-diecasting; the effect of injection velocity on the microstructure and tensile strength of this alloy have been investigated. Based on the analysis described above, the following conclusions can be drawn:

(1) The semisolid slurry of the AZ31 alloy with fine and spherical α-Mg particles of nearly 76 μm can be produced with the slurry preparation method. After rheo-diecasting, the diameter and shape factor of primary α-Mg decreased with the increase of injection velocity; meanwhile, the secondary α-Mg and eutectic mixture were refined with the increase of velocity.

(2) It was found that the formation of surface liquid segregation was closely related to the injection velocity and the solid fraction of the slurry. A high injection velocity was beneficial for reducing the surface liquid segregation. With the increase of the solid fraction, a higher injection velocity can guarantee the uniform distribution of the primary α-Mg.

(3) It was shown that casting defects such as crack and gas pores were likely to form at high injection velocities. With an increase of velocity, the size of the gas pores became smaller but the density was significantly increased.

(4) Tensile strength of the rheo-diecast AZ31 sample decreased with the increase of injection velocity. Microstructure observation of the fractured samples showed that porosity defects reduced the microstructure compactness and generated more potential nucleation sites for cracks in secondarily solidified structures between primary α-Mg phases.

Author Contributions: Formal analysis, B.X. and Y.L.; Investigation, Z.J., B.X., C.T. and J.F.; Methodology, B.X., J.F. and Y.L.; Project administration, B.X.; Writing—original draft, Z.J. and B.X.; Writing—review & editing, N.S.

Funding: This research was funded by the Zhejiang Provincial Natural Science Foundation of China (LQ16E040001).

Conflicts of Interest: The authors declare no conflict of interest.

References

1. Shahrooz, N.; Reza, G. *Semi-Solid Processing of Aluminum Alloys*; Springer: Berlin, Germany, 2016; ISBN 978-3-319-40333-5.
2. Zhao, J.W.; Xu, C.; Dai, G.Z.; Wu, S.S.; Han, J. Microstructure and properties of rheo-diecasting wrought aluminum alloy with Sc additions. *Mater. Lett.* **2016**, *173*, 22–25. [CrossRef]
3. Chayong, S.; Atkinson, H.V.; Kapranos, P. Thixoforming 7075 aluminium alloys. *Mater. Sci. Eng. A* **2005**, *390*, 3–12. [CrossRef]
4. Fu, J.L.; Wang, S.X.; Wang, K.K. Influencing factors of the coarsening behaviors for 7075 aluminum alloy in the semi-solid state. *J. Mater. Sci.* **2018**, *53*, 9790–9805. [CrossRef]
5. Eliezer, D.; Aghion, E.; Froes, F.H. Magnesium science and technology. *Adv. Perform. Mater.* **1998**, *5*, 201–212. [CrossRef]
6. Zhen, Z.; Qian, M.; Ji, S.; Fan, Z. The effects of rheo-diecasting on the integrity and mechanical properties of Mg–6Al–1Zn. *Scr. Mater.* **2006**, *54*, 207–211. [CrossRef]
7. Guan, R.G.; Zhao, Z.Y.; Dai, C.G.; Lee, C.S.; Liu, C.M.A. Novel Semisolid Rheo-Rolling Process of AZ31 Alloy with Vibrating Sloping Plate. *Mater. Manuf. Process.* **2013**, *28*, 299–305. [CrossRef]
8. Yi, M.; Shusaku, F.; Sumio, S.; Jun, Y. Cold formability of AZ31 wrought magnesium alloy undergoing semisolid spheroidization treatment. *Mater. Sci. Eng. A* **2015**, *624*, 148–156.
9. Xing, B.; Li, Y.D.; Ma, Y.; Chen, T.J.; Hao, Y. Preparation of non-dendritic microstructure of AM60 alloy for rheoforming using self-inoculation method. *Int. J. Cast Met. Res.* **2012**, *25*, 232–238. [CrossRef]
10. Xing, B.; Li, Y.D.; Feng, J.Y.; Hu, G.S.; Tang, C.L. Rheo-Cast Microstructure and Mechanical Properties of AM60 Alloy Produced by Self-Inoculation Rheo-Diecasting Process. *Metals* **2016**, *6*, 69. [CrossRef]
11. Qi, M.F.; Kang, Y.L.; Zhou, B.; Liao, W.N.; Zhu, G.M.; Li, Y.D.; Li, W.R. A forced convection stirring process for Rheo-HPDC aluminum and magnesium alloys. *J. Mater. Process. Technol.* **2016**, *234*, 353–367. [CrossRef]
12. Yan, H.; Rao, Y.S.; He, R. Morphological evolution of semi-solid Mg2Si/AM60 magnesium matrix composite produced by ultrasonic vibration process. *J. Mater. Process. Technol.* **2014**, *214*, 612–619. [CrossRef]
13. Xu, C.; Zhao, J.W.; Guo, A.; Li, H.; Dai, G.Z.; Zhang, X. Effects of injection velocity on microstructure, porosity and mechanical properties of a rheo-diecast Al-Zn-Mg-Cu aluminum alloy. *J. Mater. Process. Technol.* **2017**, *249*, 167–171. [CrossRef]
14. Guo, H.M.; Wang, L.J.; Wang, Q.; Yang, X.J. Effects of Solid–Liquid Mixing on Microstructure of Semi-Solid A356 Aluminum Alloy. *Metall. Mater. Trans. B* **2014**, *45*, 1490–1495. [CrossRef]
15. Hamasaiid, A.; Wang, G.; Davidson, C.; Dour, G.; Dargusch, M.S. Interfacial heat transfer during die casting of an Al-Si-Cu alloy. *Metall. Mater. Trans. A* **2009**, *40*, 3056–3058. [CrossRef]
16. Flemings, M.C. Behavior of metal alloys in the semisolid state. *Metal Mater. Trans. A* **1991**, *22*, 957–981. [CrossRef]
17. Guan, R.G.; Cao, F.R.; Chen, L.Q.; Li, J.; Wang, P.C. Dynamical solidification behaviors and microstructural evolution during vibrating wavelike sloping plate process. *J. Mater. Process. Technol.* **2009**, *209*, 2592–2601. [CrossRef]
18. Hitchcock, M.; Wang, Y.; Fan, Z. Secondary solidification behaviour of the Al–Si–Mg alloy prepared by the rheo-diecasting process. *Acta Mater.* **2007**, *55*, 1589–1598. [CrossRef]

19. Nangy, T.K.; Messing, R.M.; Jones, J.W.; Pollock, T.M.; Walukas, D.M.; Decker, R.F. Microstructure and properties of blended Mg-Al alloys fabricated by semisolid processing. *Met. Mater. Trans. A* **2006**, *37A*, 3725–3736.
20. Fan, Z.; Liu, G. Solidification behaviour of AZ91D alloy under intensive forced convection in the RDC process. *Acta Mater.* **2005**, *53*, 4345–4357. [CrossRef]
21. Kang, C.G.; Lee, S.M. The effect of solid fraction and indirect forging pressure on mechanical properties of wrought aluminum alloy fabricated by electromagnetic stirring. *Int. J. Adv. Manuf. Technol.* **2009**, *42*, 73–82. [CrossRef]
22. Choi, B.H.; Jang, Y.S.; Kang, B.G.; Hong, C.P. Macro-Segregation and Microstructural Characteristics in Rheo-Diecasting of a High Strength Al–4.8 mass%Si–0.7 mass%Mg Alloy. *Mater. Trans.* **2014**, *55*, 930–936. [CrossRef]
23. Khosravani, A.; Aashuri, H.; Davami, P. Liquid segregation behavior of semi-solid AZ91 alloy during back extrusion test. *J. Alloys Compd.* **2009**, *477*, 822–827. [CrossRef]
24. Mir, T.S.B.; Behzad, N. Liquid segregation behaviour of a semi-solid squeeze cast A356 aluminium cup-shaped part. *Mater. Sci. Technol.* **2017**, *10*, 1–9.
25. Vieira, E.A.; Ferrante, M. Prediction of rheological behaviour and segregation susceptibility of semi-solid aluminium–silicon alloys by a simple back extrusion test. *Acta Mater.* **2005**, *53*, 5379–5386. [CrossRef]
26. Bolouri, A.; Bae, J.W.; Kang, C.G. Tensile properties and microstructural characteristics of indirect rheoformed A356 aluminum alloy. *Mater. Sci. Eng. A* **2013**, *562*, 1–8. [CrossRef]
27. Hu, X.G.; Zhu, Q.; Midson, S.P.; Atkinson, H.V.; Dong, H.B.; Zhang, F.; Kang, Y.L. Blistering in semi-solid die casting of aluminium alloys and its avoidance. *Acta Mater.* **2017**, *124*, 446–455. [CrossRef]
28. Du, X.H.; Zhang, E.L. Microstructure and mechanical behaviour of semi-solid die-casting AZ91D magnesium alloy. *Mater. Lett.* **2007**, *61*, 2333–2337. [CrossRef]